Implication of Climate Change on Crop Water Requirement in the Semi-Arid Region of Western Maharashtra, India

Shubham Gade (shubhamgade66@gmail.com)
National Institute of Abiotic Stress Management, ICAR
Devidas Khedkar
MPKV

Research Article

Keywords: Statistical Downscaling Model, Climate change, HadCM3, Western Maharashtra, Reference crop evapotranspiration, Crop water requirement

Posted Date: October 5th, 2022

DOI: https://doi.org/10.21203/rs.3.rs-2117543/v1

Abstract

Climate change and human activities have massively impacted the hydrological cycle. Thus, it is of the greatest concern to examine the effect of climate change on water management, especially at the regional level, to understand possible future shifts in water supply and water-related crises and support regional water management. Fortunately, there is a high degree of ambiguity in determining the effect of climate change on water requirements. In this paper, the Statistical DownScaling (SDSM) model is applied to simulate the potential impact of climate on crop water requirements (CWR) by downscaling ET_0 in the region of Western Maharashtra, India, for the future periods, *viz*., the 2030s, 2050s, and 2080s, across three meteorological stations (Pune, Rahuri, and Solapur). Four crops, i.e., cotton, soybean, onion, and sugarcane, were selected during the analysis. The Penman-Monteith equation calculates reference crop evapotranspiration (ET_0). Further, in conjunction with the crop coefficient (Kc) equation, it calculates crop evapotranspiration (ETc)/CWR. The predictor variables were extracted from the NCEP reanalysis dataset for 1961–2000 and the HadCM3 for 1961–2099 under the H3A2 and H3B2 scenarios. The results indicated by SDSM profound good applicability in downscaling due to satisfactory performance during calibration and validation for all three stations. The projected ET_0 indicated an increase in mean annual ET_0 compared to the present condition during the 2030s, 2050s, and 2080s. The ET_0 would increase for all months (in summer, winter, and pre-monsoon seasons) and decrease from June to September (monsoon season). The estimated future CWR shows variation in the range for cotton (-0.97 to 2.48%), soybean (-2.09 to 1.63%), onion (0.49 to 4.62%), and sugarcane (0.05 to 2.86%).

1. Introduction

Climate change is becoming a problem and the hottest topic on the entire globe. Extreme warming caused by human emissions of greenhouse gases and the subsequent large-scale changes in weather patterns confronts climate change. Most Asian countries have witnessed more frequent floods and droughts over the last decades due to climate change and human activities (Kranz et al., 2010; Xu et al., 2013; Zhai et al., 2005). According to the 5th Assessment Report of the Intergovernmental Panel on Climate Change (IPCC), the global warming trend will continue, mainly caused by the increasing amount of greenhouse gas emissions (IPCC, 2013; Tao et al., 2015).

As per the IPCC, during the years 1880–2012, the global surface temperature rose by 0.65–1.06 ºC, and the pace of increase after 1951 was around 0.12 ºC per 10 years, which is almost double the rate since 1880 (Zhou et al., 2017). The effects of global climate change on hydrological parameters such as runoff, evapotranspiration (ET_0), surface storage, and soil moisture must be explored to determine water supply conditions (Rajabi and Babakhani, 2018; Xu et al., 2013). Global agriculture has impacted climate change in recent decades and is one of the threats to increasing food demand for the rapidly growing population under intensified environmental stress. Worldwide, a shift in the atmosphere is anticipated due to global warming and contributes to the fluctuations in CWR.

The knowledge of the water requirements of various crops is supposed to predict the water demand and the water fluctuations for effective management. Global agriculture, impacted by climate change in recent decades, is one of the main challenges of rising food supply for the rapidly growing population. The regional cropping calendar, cropping system, growing season, crop water requirement (CWR), and irrigation requirement (IR) for different agro-climatic zone rely on the respective climatic parameters such as precipitation, temperature, relative

humidity, evapotranspiration, wind speed, sunshine hours, etc. (Goyal, 2004; Thomas, 2008). It was analyzed that seasonal rainfall (June-Sept) in Maharashtra directly impacted soil moisture variation (Gade et al., 2021). Furthermore, the agriculture sector and CWR are more sensitive to and affected by climate variability through extreme climate events such as droughts, floods, and heatwaves.

Past studies (IPCC, 2013, 2007, 2002; Pandey et al., 2008) revealed that worldwide precipitation, temperature, evapotranspiration, wind speed, and sunshine hours fluctuated from normal in the last century. These are due to both natural as well as anthropogenic factors. Temperature is the prime climatic variable for the water allocation and farming sector after precipitation (Duhan et al., 2013). Studies have also shown that temperature levels are rising with higher latitudes in the Northern Hemisphere (Kumar, 2007). (Goyal, 2004) conducted a sensitivity analysis of the evapotranspiration rate over Rajasthan, India. The results suggested that the evapotranspiration rate rose by 14.8%, with a significant increase in temperature by 20%.

Crop evapotranspiration (ETc) varies significantly from ET_0 as soil cover, canopy properties, and aerodynamic resistance. Due to alterations in crop characteristics during the growing season, the crop coefficients change from sowing to harvesting. As a result, different crops would have different crop coefficients. The crop coefficient also influences the varying properties of the crop during its growth. Penman-Monteith (P-M) is still the only standard method under all climatic conditions recommended by FAO 56 (Allen et al., 1998). Potential climate change significantly affects agriculture and water supplies; in a nutshell, the crop production sector should be more conscious of productive approaches for the application and storage of water. (Doria et al., 2006) have demonstrated that simulation reliant on both natural and anthropogenic radiative forcing is more closely associated with observed data, which only accounts for natural climatic conditions.

Many downscaling methodologies have been proposed in the last two decades, recognizing the temporal and spatial mismatch between the regional and gross scales. These techniques were mainly used in Europe and the United States (Wilby and Wigley, 1997). By deriving regional climate detail from global climate data (Gagnon et al., 2005), downscaling approaches have emerged as effective methods to reduce the problem of indistinct scales. Various researchers (Guo et al., 2018; Kundu et al., 2017; Manasa and Shivapur, 2016; Tao et al., 2015; Wang et al., 2013; Xu et al., 2014; Zhou et al., 2017) downscaled ET_0 using SDSM and other models and found significant variations in contrast to current conditions. The statistical downscaling is based on a few assumptions; the predictor–predictand relationships are valid under future climatic conditions, and predictor variables with their changes are well characterized by GCMs (Saraf and Regulwar, 2016; Wilby and Wigley, 2000). Studies in the Tibetan plateau by (Wang et al., 2013) projected ET_0 during 2011–2100 from the HadCM3 and CGCM3 models, where SDSM performed satisfactorily in downscaling ET_0, and the continuous increment in ET_0 was observed in the 21st century. (Guo et al., 2018) analyzed the evaluation indices (R2, *Ens*) during the calibration and validation periods. The results indicated a fair simulation of temperature and evapotranspiration by the SDSM model. The SDSM combines multiple regression and a stochastic weather generator (Gebremeskel et al., 2004; Mahmood and Babel, 2013).

Although climate projections of rainfall and temperature are frequent, there has been limited research on the generation of future ET_0 (Kundu et al., 2017). However, ET_0 is not only a crucial climatic parameter controlling the water balance but also a key factor influencing crop production. In the semi-arid areas of less rainfall or rainfall-based agricultural seasons (such as Western Maharashtra), variation in crop water requirements may

create a problem. The future projection of ET_0 has not been made in the region. Therefore, it is necessary to study variations in ET_0 and evaluate their effectiveness in the future, and develop better management strategies.

2. Materials And Methods

2.1. Study area description

The investigation was carried out for the region of Western Maharashtra, the agro-climatic region of Maharashtra in the western province of India. The major crops grown in the study area are cotton, onion, soybean, sugarcane, groundnut, sorghum, and maize. The average annual rainfall in the region ranges from 608–635 mm. The climate of Western Maharashtra is hot and dry. 89% of annual rainfall in the central part during southwest monsoon rainfall is received from June to September, with 37 rainy days out of 122 days having daily rainfall (r > = 2.5) (Guhathakurta et al., 2020). The average annual rainfall decreases from 852 mm on the southern side to 567.5 mm on the northern side (TERI, 2014). Western Maharashtra is more irrigated than the rest of Maharashtra. The geology of the region is dominated by basaltic rock. The study area occupied the largest share (50 percent) of the gross irrigated area of the state since most of the rivers originate from the Western Ghats mountain ranges and are diverted to the east through Western Maharashtra. The irrigation potential of 4.826 × 106 ha-m has been created by the Water Resources Department of the state through 3,712 completed and ongoing projects (Audit, 2018). The conditions adversely affect the socio-economic conditions of the people, mainly dependent on agriculture. It also has a phenomenal impact on crop water requirements.

2.2. Location of study area

The area for the study is in the Western Maharashtra region bounded by latitudes 17º 39' to 19º 24' N and 73º 50' to 75º 55' E. The selected regional stations with their names, latitude, longitude, and altitude are represented in Table 1. The boundary map of the study area with selected stations is depicted in **Fig. 1**.

Table 1 The details of the meteorological stations under the study area

Sr. No	District	Station	Latitude	Longitude	Altitude	Data
1.	Ahmednagar	Rahuri	19^0 23' 33"N	74^0 38' 56"E	514.55 m	1975–2000
2.	Pune	Pune	18^0 31' 13"N	73^0 51' 24"E	559.90 m	1970–2000
3.	Solapur	Solapur	17^0 40' 08"N	75^0 54' 24"E	483.50 m	1967–2000

2.3. Data Acquisition

2.3.1. Geographical Data:

2.3.2. Meteorological Data:

The climatic parameters such as maximum temperature, minimum temperature, maximum relative humidity, minimum relative humidity, bright sunshine hours, and wind speed were used to estimate reference crop

evapotranspiration. The data was acquired from the Indian Meteorological Department (IMD), Pune, and SAU, Rahuri, for selected stations. It was available as a continuous record in a daily format.

2.3.3. Reanalysis Data:

The estimation of future crop water requirements was done by analyzing NCEP and GCM data along with observed meteorological data of the study area. The National Centre for Environmental Prediction (NCEP) provides daily reanalysis data of 26 factors. These include mean temperature, mean sea level pressure, near-surface relative humidity, near-surface specific humidity, 500 hPa geopotential height, 850 hPa geopotential height, and relative humidity, geostrophic airflow velocity, vorticity, zonal velocity component, meridional velocity component, wind direction and divergence at the surface, 500 hPa height, and 850 hPa height (Zhou et al., 2017). Table 5 describes the predictors along with their descriptions. The grid resolution is 2.5 degrees of latitude by 2.5 degrees of longitude. This data is available on the Canadian Climate Impact Scenarios (CCIS) website (Guo et al., 2018).

2.3.4. GCM Data:

The General circulation model (GCM) data was used for generating different scenarios. The GCM selected was the Hadley Centre Coupled Model version 3 (HadCM3). The HadCM3 is a coupled climate model with a horizontal resolution of 2.5 degrees of latitude by 3.75 degrees of longitude, and the predictors were the same as in NCEP data. The predictor variables are available for 1961–2099 (Saraf and Regulwar, 2016). Furthermore, this model has been extensively used in the statistical downscaling of climatic variables across the Indian sub-continent (Anandhi et al., 2008; Mahmood and Babel, 2013; Saraf and Regulwar, 2016). The output of HadCM3 consists of two scenarios (H3A2 and H3B2), both used in the study.

2.4. Estimation of Crop Water Requirement (CWR)

The estimation of CWR is one of the basic needs for crop planning of any irrigation project. The water requirement is specified as the quantity of water, regardless of its source, needed by a crop or diversified crop pattern for its growth under field conditions in a given period (Micheal, 2008). The water requirement encompasses losses due to crop evapotranspiration (ETc) or consumptive use (Cu). In addition to losses during water use (inevitable losses), seepage losses also occur.

$$WR = ET_c \text{ or } C_u + \text{application losses} \quad \text{.... (1)}$$

The water requirement for plants is, therefore, a "demand" and a "supply" consisting of a contribution from any source of water, the primary source being irrigation water (IR), effective rainfall (ER), and soil profile contribution (S). Here, water requirement was estimated considering the demand side and nullifying the losses due to application as these parameters vary from place to place. The following relationship calculates the crop evapotranspiration,

$$ET_C = ET_0 \times K_C \quad \text{.... (2)}$$

Where, ET_c = Crop evapotranspiration (mm/day); ET_0 = Reference crop evapotranspiration (mm/day); and K_c = Crop coefficient (dimensionless)

ET_0 was calculated using the FAO 56 Penman-Monteith method (Allen et al., 1998). It is recommended as the sole method for determining ET_0 and is represented as:

$$ET_0 = \frac{0.408*\Delta*(R_n-G)+\gamma*\left(\frac{900}{T+273}\right)*U_2*(e_s-e_a)}{\Delta+\gamma*(1+0.34*U_2)} \quad \text{.... (3)}$$

Where, ET_0 = Reference crop evapotranspiration (mm/day); Δ = Slope of saturation vapour pressure temperature curve (kPa/^{0}C); γ = Psychometric constant (kPa/^{0}C); T = Mean air temperature (^{0}C); e_s= Saturated vapour pressure (kPa); e_a= Actual vapour pressure (kPa); R_n= Net radiation (MJ/m^2/day); G = Soil heat flux density (MJ/m^2/day); U_2 = Wind speed at 2m height (m/s) and (e_s - e_a) = Saturated vapour pressure (kPa)

The net radiation was estimated as follows:

$$R_n = 0.77\left(a + b\frac{n}{N}\right)R_a - R_{nl} \quad \text{.... (4)}$$

Where, a and b are empirical coefficients (a = 0.18 and b = 0.55); *n (h)* is the sunshine duration; *N* (h) is the maximum sunshine duration; R_a (MJ/m^2.d) is the extraterrestrial radiation; and R_{nl} (MJ/m^2.d) is the net outgoing longwave radiation (Wang et al., 2019; Zotarelli et al., 2010).

2.4.1. Details of Selected Crops

For estimation of crop water requirement, cotton, onion, soybean, and sugarcane crops were selected as they are majorly grown in the study region. The details of selected crops for analysis with their growth period, duration, and season are described in Table 2.

Table 2
Details of selected crop with growth period

Crops	Sowing Date	Harvesting Date	Duration	Season
Cotton	15 May	10 Nov.	180 Days	*Kharif*
Onion	15 Oct.	11 Feb.	120 Days	*Rabi*
Soybean	1 July	8 Oct.	100 Days	*Kharif*
Sugarcane	30 Jan.	29 Jan.	365 Days	*Perennial*

2.4.2. Crop Coefficient (Kc) Equations

The crop coefficient varies with crop growth stages. The Kc values were interpolated for the initial, mid-season, and late-season stages. The daily Kc values for different crops in the Rahuri region during their entire growth were calculated by the polynomial equations generated by the Department of Irrigation and Drainage Engineering and recommended by Mahatma Phule Agriculture University, Rahuri (India). It was assumed that the equations

are valid over the entire study area and do not change concerning place and time. The details of the Kc equation for cotton, onion, soybean, and sugarcane are well-illustrated below in Table 3 and Fig. 3, where t = Day since sowing; T = Total crop growth period in days.

Table 3
The Kc equation for cotton, onion, soybean and sugarcane

Crops	Polynomial equation
Cotton	$K_{ct} = 18.78 * \left(\frac{t}{T}\right)^4 - 39.98 * \left(\frac{t}{T}\right)^3 + 24.06 * \left(\frac{t}{T}\right)^2 - 2.89 * \left(\frac{t}{T}\right) + 0.453$
Onion	$\mathrm{K_{ct}} = 8.062 * \left(\frac{t}{T}\right)^5 - 24.31 * \left(\frac{t}{T}\right)^4 + 20.15 * \left(\frac{t}{T}\right)^3 - 5.76 * \left(\frac{t}{T}\right)^2 + 1.498 * \left(\frac{t}{T}\right) + 0.561$
Soybean	$K_{ct} = 2.647 * \left(\frac{t}{T}\right)^5 + 0.14 * \left(\frac{t}{T}\right)^4 - 8.76 * \left(\frac{t}{T}\right)^3 + 5.862 * \left(\frac{t}{T}\right)^2 + 0.26 * \left(\frac{t}{T}\right) + 0.494$
Sugarcane	$\mathrm{K_{ct}} = 0.484 * \left(\frac{t}{T}\right)^4 - 4.948 * \left(\frac{t}{T}\right)^3 + 3.988 * \left(\frac{t}{T}\right)^2 + 0.636 * \left(\frac{t}{T}\right) + 1.498$

2.5. Estimation of Future Crop Water Requirement

General circulation models (GCMs) can very well predict the significant characteristics of the projected climate on a wide scale in the study of regional climate change. However, GCMs have limited utility due to their poor spatial resolution and lack of regional climate information. There are two ways to compensate for GCMs' inadequacy in projecting regional climate change: to create new GCMs with higher resolution and downscale GCMs to the regional scale. The Downscaling techniques are categorized further into Dynamic DownScaling and Statistical DownScaling. The purpose of dynamical downscaling is to build a regional climate model with a clear physical meaning that will not be affected by the observation data. However, it also has some disadvantages. For example, the requirement for significant computing resources is not readily transferred to new regions or domains. Statistical downscaling is premised on the theory that the large-scale climatic state and local physiographic factors influence regional climate (Zhou et al., 2017).

The SDSM, developed by R. L. Wilby and C. W. Dawson, started its life in the summer of 2000. It is a combination of multiple linear regression (MLR) and stochastic weather generator (SWG) (Wilby et al., 2002). MLR is used to build an empiric relationship between predictors (NCEP) and predictands (observed local scale data) and develop regression parameters. A stochastic weather generator (SWG) simulates up to 100 daily time series from predictors of NCEP and GCMs based on the regression parameters (Mahmood and Babel, 2013).

3.6 Theoretical Consideration of SDSM

The SDSM (Statistical DownScaling Model) is a decision support method for evaluating local climate change impacts using a rigorous statistical downscaling approach. In addition, the program performs ancillary tasks of

variable pre-screening, model calibration, basic diagnostic testing, statistical analysis, and graphing of climate data.

The statistical downscaling technique utilized in this study was SDSM version 4.2 (Wilby and Dawson, 2007) to simulate crop evapotranspiration for future periods centered on the 2030s, 2050s, and 2080s. The step-by-step procedure using SDSM is summarized further.

The National Center for Environmental Prediction (NCEP) relates the intensity of each predictor-predict relationship; the calibration and validation stage facilitate the establishment of statistical relationships between the selected predictors and the surface predictand (Gagnon et al., 2005). In this process, simulation of observed data was done with predictors from the re-analysis of NCEP data, while for the 2030s, 2050s, and 2080s global climate models, HADCM3 with emission scenarios H3A2 and H3B2.

Table 4
Climatic scenario classes

Scenario Classes	Concerns	Remarks
A2	• Rapid economic growth • Low population growth • Rapid new technology • Concern to wealth rather than environment	• Homogenous world on economic development • Cultural convergence • No difference in per capita income
B2	• Diverse technological change • Emphasis on community initiative • Concern on environment rather than economic development	• Heterogeneous world • Local solutions for environmental and social sustainability

The IPCC has grouped future emission scenarios into four significant classes/groups: a) A1, b) A2, c) B1, and d) B2, based on the level of economic development and environmental concern. It is to be observed (Table 4) that the scenario group or class A2 is concerned more about activities that will improve the world's economic development. In contrast, B2 is more concerned about the world's environmental sustainability (Mohan and Ramsundram, 2014).

Table 5
Details of predictors used in the present study

Sr. No	Predictor	Description
1	p_f	Surface airflow strength
2	p_u	Surface zonal velocity
3	p_v	Surface meridional velocity
4	p_z	Surface velocity
5	p_th	Surface wind direction
6	p_zh	Surface divergence
7	rhum	Surface relative humidity
8	p5_f	500 hPa airflow strength
9	p5_u	500 hPa zonal velocity
10	p5_v	500 hPa meridional velocity
11	p5_z	500 hPa vorticity
12	p5th	500 hPa wind direction
13	p5zh	500 hPa divergence
14	r500	500 hPa relative humidity
15	p8_f	850 hPa airflow strength
16	p8_u	850 hPa zonal velocity
17	p8_v	850 hPa meridional velocity
18	p8_z	850 hPa vorticity
19	p8th	850 hPa wind direction
20	p8zh	850 hPa divergence
21	r850	850 hPa relative humidity
22	p500	500 hPa geopotential height
23	p850	850 hPa geopotential height
24	temp	Mean temperature at 2m height
25	shum	Surface-specific humidity
26	mslp	Mean sea level pressure

The GCM outputs used in the analysis are derived from the United Kingdom Meteorological Office's Hadley Center Coupled Ocean/Atmosphere Climate Model, version 3 (HadCM3). It includes A2 (high greenhouse gas emissions) and B2 (low greenhouse gas emissions) scenarios with a daily time series from 1961 to 2099.

Similarly, the NCEP reanalyzed dataset is a daily time series from 1961 to 2000, including 26 large-scale weather factors. Table 5 represents the variable number, the abbreviation, and the description of the 26 GCM or NCEP weather factors.

The downscaling process involved the following steps: quality check of data, the transformation of data, screening of predictors, calibration of sub-model using observed data (predictand) and selected NCEP predictors, generation of present and future scenarios from gridded datasets of NCEP and GCMs, and statistical analysis.

2.5.1. Quality Control Check and Transformation of Observed Data (Predictand)

The meteorological stations might have anomalies or missing records following this quality control check function verifies the dataset. The missing data is replaced with the identifier value/code, i.e., -999. The second step after the quality control check is the transformation of data. SDSM can convert data before calibration into various formats such as logarithm, power, inverse, and binomial (Saraf and Regulwar, 2016).

2.5.2. Selection of Large-Scaled Predictor

The selection of predictors is a crucial step in the statistical downscaling process. Their four rules govern the selection of predictors (Amin et al., 2014; Guo et al., 2018) stated below

1. There is a strong correlation and agreement between predictor and predictand.
2. The selected predictor can be simulated by the GCM.
3. The selected predictors should maintain independence or weak dependence.

A screening of predictor variables chose the predictors of the SDSM model. The strongly associated and correlated predictors were screened using correlation analysis, scatter plots, and seasonal variance methods of the SDSM model. The number of control predictors in the recursive algorithm adopted by SDSM is limited to 12, while the predictors in GCM or NCEP are typically more than 20, making the correlation screening analysis more complicated to perform in one stage. After selecting the large-scale predictor, the predictors from the reanalysis data (NCEP) and predictand (observed station) data were used to establish the statistical relationships for the study area.

2.5.3. Selection of sub-model

There are also two sub-models: conditional and unconditional; depending on the local-scale variables either can be used. The unconditional sub-model is used for independent variables such as temperature, evapotranspiration, and sunshine hours (Chu et al., 2010; Gagnon et al., 2005; Hussain et al., 2015; Mahmood and Babel, 2013; Saraf and Regulwar, 2016; Wilby and Wigley, 2000). The default permits unconditional processes in the downscaling model to simulate negative values (e.g., minimum temperature); deselection truncates values at zero (e.g., sunshine hours). This default does not affect conditional processes (rainfall). In unconditional models, a direct relationship between predictors and predictands is assumed (e.g., local wind speeds may be a function of regional airflow indices). In conditional models, there is an intermediate process between regional forcing and local weather (for example, local precipitation quantities are determined by the occurrence of rainy days, which are determined by regional-scale predictors such as humidity and atmospheric pressure) (Wilby and Wigley, 2000, 1997).

Precipitation and evaporation are dependent variables under the conditional sub-model. The distribution of precipitation data is typically non-normal, although evapotranspiration data follows a normal distribution. In SDSM, specific data transformation can be applied to the conditional model. In the conditional sub-model, thresholds can be defined to exclude values less than or equal to the event threshold. Before using the data in regression equations, SDSM can convert it to make it normal (Hussain et al., 2015; Khan et al., 2006). Several statistical parameters (generic and conditional tests) and graphical assessment techniques (such as bar plots) are used in SDSM to assess the performance (Gebrechorkos et al., 2019). In the present study, an unconditional sub-model was used without transformation and optimization of the best fit by ordinary least square (OLS).

2.5.4. Calibration and Validation of Model

The ET_0 was calibrated and validated based on the available observed daily data. The model was developed using the monthly sub-model and selected NCEP predictors. As per the availability of data, NCEP, H3A2, and H3B2 predictors simulated the model for 1968–2000, 1970–2000, and 1975–2000 for Solapur, Pune, and Rahuri stations, respectively. A total of 20 ensembles were generated for the monthly SDSM and used in the study (Mahmood and Babel, 2013). The SDSM can generate up to 100 ensembles and can be used to research the uncertainty analysis of climate scenarios (Saraf and Regulwar, 2016). The total dataset was utilized as follows: 2/3rd of the total data was for calibration, and 1/3rd of the remaining data was for validation. The calibration periods for Pune, Rahuri, and Solapur were 1970–1990, 1975–1990, and 1968–1989, respectively. In contrast, the validation periods for Pune, Rahuri, and Solapur were 1991–2000, 1991–2000, and 1990–2000, respectively.

2.5.5. Statistical analysis for model performance

The statistical parameters evaluated the performance of SDSM for all three stations during the calibration and validation (Huang et al., 2011; Mahmood and Babel, 2013). These parameters are mean (μ), coefficient of determination (R^2), nash-sutcliffe evaluation (*Ens*), root mean square error (RSME), standard deviation (SD), standard error in mean (SE- μ), mean absolute deviation (MAD) and mean absolute percentage error (MAPE). The general equations of all statistical terms are described below.

(1) Coefficient of determination (R^2)

The coefficient of determination was used to show the model's accuracy in predicting data. The coefficient of determination (R2) is presented as.

$$R^2 = \frac{\sum(X_i - X')*(Y_i - Y')}{\sqrt{\sum(X - X')^2 * (Y - Y')^2}} \quad (8)$$

The value of R^2 explains the correlation between observed and downscaled values. It lies between 0 and 1, where 0 indicates poor, and one indicates the best.

(2) Nash-Sutcliffe evaluation (E_{ns})

The Nash-Sutcliffe (*Ens*) evaluation index (Eq. 9) was used to assess the model applicability by comparing observed data with the output of SDSM.

$$E_{ns} = 1 - \frac{\sum_{i=1}^{n}(X_i - Y_i)^2}{\sum_{i=1}^{n}(X_i - X')^2} \quad \text{.... (9)}$$

Xi and *Yi* are time-series of observed value *X* and simulated value *Y*; and *X'*, *Y'* is the mean of observed value *X* and simulated value *Y*. The Nash-Sutcliffe (*Ens*) index ranges from $-\infty$ to 1; the closer the model efficiency is to 1, the more accurate (Guo et al., 2018).

(3) Root Mean Square Error (RMSE)

The Root Mean Square Error (RMSE) is a measure of the difference between values predicted by a model and the values observed in the environment that is being modeled.

$$RMSE = \sqrt{\frac{\sum_{i=1}^{n}(X_{obs,i} - Y_{mod,i})^2}{n}} \quad \text{.... (10)}$$

Where $X_{obs,i}$ are observed value and $Y_{mod,i}$ are projected modelled value.

(4) Mean Absolute Percentage Error (MAPE)

The Mean Absolute Percentage Error (MAPE) measures the prediction accuracy of a forecasting method. It measures the size of the error in percentage terms. The statistical formula of MAPE is given in Eq. 11.

$$MAPE = 100 * \frac{1}{n} * \sum_{i=1}^{n} \left| \frac{X_i - Y_i}{X_i} \right| \quad \text{.... (11)}$$

Where X_i and Y_i are individual values of observed and modelled data respectively.

(5) Mean Absolute Deviation (MAD)

The Mean Absolute Deviation (MAD) of a data set is the average distance between each data value and the mean. A dataset's mean absolute deviation is a way to describe variation in a data set. The statistical formula of MAPE is given in Eq. 12.

$$MAD = \frac{\sum|(X - X')|}{n} \quad \text{.... (12)}$$

(6) Standard Error Mean (SE- μ) and Standard Deviation (SD)

The Standard Error in mean (SE- μ) was used to observe the variability of the data predicted by the model and was given by Eq. 13. The Standard Deviation (SD) is a measure of variability or the scatter or the dispersion of the mean value.

$$SE = \sqrt{\frac{\sum_{i=1}^{n}(Y' - X')^2}{n}} \quad \text{.... (13)}$$

Where *n* is the number of time series and other notation same as above.

$$SD = \sqrt{\frac{\sum_{I=1}^{N}(X_i - X')^2}{N}} \quad \text{.... (14)}$$

Where, *Xi* is variable, *X'* is mean, and N is total number of variables

2.5.6. Generation of Present and Future Time Series for Reference crop evapotranspiration (ET_0)

Following calibration and validation of the model, the weather generator function was applied to generate a synthesis daily time series of ET_0 presenting climate from a selected set of NCEP predictors. The generated daily time series of ET_0 was compared statistically with the observed records to check how close it was to the present climate. Finally, the scenario generator function was used to stimulate future time series of ET_0 using output from GCMs (HadCM3) under H3A2 and H3B2 scenarios.

Daily ET_0 data for the observed period for the mentioned stations was provided in (.DAT) format to the SDSM model, and the model input files have been established. The downscaled data per requirements was simulated for three future periods based on the base period. As discussed earlier, downscaling was done for three time periods, the 2030s, 2050s, and 2080s, depending on the observed data period.

Considering Solapur station

The observed data was available for 33 years. The years were split as (16 + 1 + 16), where the first 16 are considered pre-years and the next 16 as post-years. Thus, the analysis period for the 2030s was 2014–2046, keeping the year 2030 at the center. A similar procedure was adopted for the 2050s, 2080s, and remaining stations (Table 6).

Table 6
Analysis period/time for projecting future scenarios in **ET_0**

Periods	Solapur	Pune	Rahuri
Base/Observed Period	1968–2000	1970–2000	1975–2000
First period (2030s)	2014–2046	2015–2045	2017–2043
Second period (2050s)	2034–2066	2035–2065	2037–2063
Third period (2080s)	2064–2096	2065–2095	2067–2093

The steps involved in downscaling and scenario generation is shown in Fig. 3.

3. Results

The study analyzed variability in crop water requirements for future atmospheric conditions. The daily ET_0 was calculated using the Penman-Monteith equation discussed in section 2.4. The output of daily ET_0 was used for projecting future ET_0 during different periods. The projected ET_0, in combination with crop coefficient (Kc), calculated CWR for future periods, and further variation in crop water requirement was analyzed using observed data. Based on base climate data, the SDSM was used to project future ET_0 for three periods: the 2030s, 2050s, and 2080s. The analysis results were presented separately for Pune, Rahuri, and Solapur stations. The performance of SDSM model predictions was studied using observed and predicted values of ET_0 during the same period.

3.1. Screening of predictors

The selection of predictors was a crucial step in the downscaling process. It is an iterative procedure consisting of a rough screening of the predictors repeated until an objective function is optimized (Wilby and Harris, 2006). The variables with the highest correlation were selected using the screen variable tool in the SDSM. Initially, all the predictors from historical records were correlated with the observed data of ET_0. The predictors with the highest correlation were chosen with a minimum (or zero) p-value and a maximum partial r-value. The correlation statistics and p-values explain the strength of the relationship between the predictor and predictand and multi-co-linearity among selected predictors. The number of selected predictors varied from three to four. The correlations with a p-value (< = 0) were selected to predict results better. Table 7 represents the selected predictors and the partial r value for ET_0.

Table 7
Selected predictors with partial r values for reference crop evapotranspiration (ET_0)

Sr. No.	Predictors	Meteorological stations with partial r values		
		Pune	Rahuri	Solapur
1	nceptempas	0.494	0.362	0.337
2	ncepp_zhas		0.260	0.245
3	ncepp_uas	0.185	0.243	
4	ncepp5_uas	0.244		
5	ncepp8_uas			0.101
6	ncepp8_vas		0.124	0.056

(Suo et al., 2019) examined partial r values for temperatures ranging from 0.27 to 0.77. Similarly, identical partial r values for temperature and precipitation were also observed by Mahmood and Babel, 2013. The highest correlation values represent a higher degree of association, while smaller p-values describe a better chance of association between variables. The selection of predictors was made as discussed in section 2.5.2. Amongst 26 predictors, only six (nceptempas, ncepp_zhas, ncepp_uas, ncepp5_uas, ncepp8_uas, and ncepp8_vas) were used as they strongly correlated with observed (ET_0) (Table 7). For all three weather stations, nceptempas (the temperature at 2 m height) was a super predictor and common to all three stations with the highest "partial r"

value. A similar super-predictor (nceptempas) in the downscaling of ET_0 for nine stations in the Beijing region was also examined by (Guo et al., 2018).

3.2. Calibration and Validation of Model

The Calibrate Model operation takes a user-specified predictand with a set of predictor variables and computes the parameters of multiple regression equations via an optimization algorithm (ordinary least squares). Before future scenario construction, the results of the observed data of ET_0 were correlated with the modeled data during the calibration and validation. All measured statistical values conspicuously resembled the statistics of observed data for ET_0.

Table 8
Statistical criteria for best fit model for downscaling ET_0 during calibration for HadCM3 model

Pune (1970–1990)								
Data type	**R^2**	E_{ns}	**RMSE**	**MAPE**	**μ**	**S.D.**	**SE-μ**	**MAD**
OBS	-				4.583	1.39	0.016	1.38
NCEP	0.71	0.713	0.92	16.10	4.575	1.05	0.012	1.21
H3A2	0.72	0.719	0.91	16.12	4.584	1.07	0.012	1.22
H3B2	0.72	0.721	0.90	16.09	4.574	1.06	0.012	1.23
Rahuri (1975–1990)								
Data type	**R^2**	E_{ns}	**RMSE**	**MAPE**	**μ**	**S.D.**	**SE-μ**	**MAD**
OBS	-				5.087	1.47	0.019	1.44
NCEP	0.69	0.685	1.000	15.86	5.073	1.10	0.014	1.23
H3A2	0.68	0.683	1.003	15.93	5.080	1.12	0.015	1.24
H3B2	0.68	0.683	1.002	15.84	5.078	1.13	0.015	1.24
Solapur (1968–1989)								
Data type	**R^2**	E_{ns}	**RMSE**	**MAPE**	**μ**	**S.D.**	**SE-μ**	**MAD**
OBS	-				5.709	1.73	0.019	1.61
NCEP	0.60	0.603	1.32	18.33	5.689	1.27	0.014	1.39
H3A2	0.61	0.609	1.31	18.19	5.690	1.25	0.014	1.39
H3B2	0.61	0.609	1.31	18.16	5.694	1.27	0.014	1.38

The SDSM showed the best values of all performance measures, higher values for R2 and *Ens* and lower values for RMSE and MAPE. The MAD values show that there was consistently less variation among observed and downscaled data, ranging from 1.2 to 1.6 mm. The analysis also pointed out that the performance measures as

R2 and *Ens* were more than 0.71, 0.68, and 0.60 for Pune, Rahuri, and Solapur stations, respectively. The values of RMSE varied from 0.90 to 0.92 for Pune, 1.000 to 1.003 for Rahuri, and 1.31 to 1.32 mm for Solapur station.

Similarly, it was worth noticing that for calibration, MAPE was less than 16.12, 15.93, and 18.33% for Pune, Rahuri, and Solapur stations. The mean, standard deviation, and standard error mean suggested that observed and modeled data had an almost similar mean, less deviation, and less error between observed and predicted values.

Table 9
Statistical criteria for best fit model for downscaling ET_0 during validation for HadCM3 model

Pune (1991–2000)								
Data type	**R^2**	E_{ns}	**RMSE**	**MAPE**	**μ**	**S.D.**	**SE-μ**	**MAD**
OBS	-				4.452	1.62	0.027	1.30
NCEP	0.70	0.698	0.89	15.96	4.442	1.38	0.023	1.15
H3A2	0.70	0.698	0.89	15.78	4.434	1.39	0.023	1.16
H3B2	0.70	0.701	0.88	15.68	4.442	1.40	0.023	1.16
Rahuri (1991–2000)								
Data type	**R^2**	E_{ns}	**RMSE**	**MAPE**	**μ**	**S.D.**	**SE-μ**	**MAD**
OBS	-				4.221	1.44	0.024	1.17
NCEP	0.71	0.71	0.78	14.48	4.201	1.22	0.020	0.98
H3A2	0.70	0.70	0.79	14.51	4.211	1.23	0.020	0.99
H3B2	0.71	0.71	0.78	14.37	4.196	1.24	0.020	1.00
Solapur (1990–2000)								
Data type	**R^2**	E_{ns}	**RMSE**	**MAPE**	**μ**	**S.D.**	**SE-μ**	**MAD**
OBS	-				4.850	1.67	0.026	1.35
NCEP	0.62	0.61	1.11	18.51	4.842	1.37	0.022	1.14
H3A2	0.62	0.61	1.12	18.56	4.849	1.36	0.021	1.15
H3B2	0.61	0.61	1.10	18.43	4.836	1.36	0.021	1.15

Similarly, Table 9 represents statistical performance during the validation period. In the Rahuri station, considering NCEP data, the value of the R2 and *Ens* was 0.71 in the validation stage. There were lesser values of RMSE and MAPE at 0.78 and 14.48, respectively. There was an identical close difference during the calibration and validation period for each performance measure of the remaining HadCM3 data (H3A2 and H3B2 scenarios) for the Pune and Solapur stations.

Overall, the performance suggests that for the accurate projection of ET_0, HadCM3 data is a valid approach. Based on Tables 8 and 9, the derived predictor–predictand relationships were considered satisfactory for three stations. Guo et al. 2018 observed that the values of R2 and *Ens* ranged from 0.61 to 0.78 during the calibration and validation of downscaled ET_0 in China. Similar values of R2 were also observed by Saraf and Regulwar 2016 during the calibration of observed and modeled temperature for the Godavari basin, Maharashtra (India).

3.3. Projected Changes in ET_0 for Future Climate Scenarios

The changes in mean monthly ET_0 in the three selected stations under all scenarios would present noticeable differences in other months.

3.3.1. Future projections and percent change in ET_0 for Pune station

Figure 4a and b represented the changes in ET_0 for future 2030s, 2050s, and 2080s relative to the base period (1970–2000) under H3A2 and H3B2 scenarios for Pune stations. The figure represents general monthly changes observed in modeled ET_0. It showed that the changes in ET_0 projected under both scenarios were quite different in magnitude (amount) but identical in pattern. The maximum mean monthly ET_0 (7.43 mm) for the base period was observed in May, whereas the minimum ET_0 was 3.08 mm in December. Projected ET_0 presented an increasing trend in the entire period from 2015 to 2095 under both scenarios during the 2030s, 2050s, and 2080s. The maximum projected ET_0 would be in May, followed by April during the 2030s, 2050s, and 2080s, whereas the minimum projected ET_0 would be in December, followed by August.

During the 2050s and 2080s periods, there would be an increment in the average ET_0 for all months except June and August. The maximum decrease in mean monthly ET_0 for the 2050s would be in August (-9.15%) under the H3A2 and − 8.78% under the H3B2 scenario. In August 2080s, ET_0 would moderate by -3.81 and − 7.36% under the H3A2 and H3B2 scenarios, respectively, observed in Fig. 4c and d.

In the long-term seasonal trend analysis of ET_0, a decreasing trend was observed in the monsoon period (m = -0.188 mm season^{-1} year^{-1}). In contrast, an increasing trend was observed during the northeast winter monsoon (m = 0.156 mm season^{-1} year^{-1}) and pre-monsoon (m = 0.068 mm season^{-1} year^{-1}) periods (Goroshi et al., 2017). Tamaddun et al. 2019 found a similar decrease in PET during the post-monsoon months in India. The above references support for the similar outcome of decreased ET_0 in August and September.

3.3.2. Future projections and percent change in ET_0 for Rahuri station

ET_0 constantly advanced over three periods at Rahuri station, with a maximum increasing rate in contrast to the baseline period computed for the 2080s. The max and min mean monthly ET_0 during the base period were observed in May (7.54 mm) and December (2.98 mm), respectively. The maximum projected ET_0 during the

2030s, 2050s, and 2080s would be in May, followed by April, whereas the minimum projected ET_0 would be in December, followed by November, Fig. 5(a and b). The percentage change in ET_0 for Rahuri station revealed variation in the range for 2030s (-3.24 to 5.04%), 2050s (-4.73 to 5.59%), and 2080s (-5.96 to 12.39%) under the H3A2 scenario, whereas, in the range for 2030s (-4.91 to 4.92%), 2050s (-6.40 to 7.23%), and 2080s (-6.49 to 8.52%) Fig. 5(c and d). Kundu et al. 2017 observed an increase in projected ET_0 with both increase and decrease fluctuations during different decades, with the highest rise projected in 2091–2099, particularly in the winter season from November to January.

3.3.3. Future projection and percent change in ET_0 for Solapur station

Solapur station had higher mean monthly ET_0 values for all months than Rahuri and Pune stations. The maximum and minimum mean monthly ET_0 during the base period were in May (8.25 mm) and December (3.90 mm), respectively (Fig. 6a and b). The maximum projected ET_0 would be in May, followed by April, whereas the minimum ET_0 would be in December, followed by November.

The Solapur station would show increments of 1.76, 2.01, and 2.73% under the H3A2 scenario and 1.54, 2.52, and 3.13% under the H3B2 scenario during the periods of 2030s, 2050s, and 2080s, respectively for mean annual values (Fig. 6c and d).

Overall, for most of the months, it was envisioned that a gradual rise in projected ET_0 during the 2030s, 2050s, and 2080s periods. The maximum and minimum mean monthly projected ET_0 would be observed in May and December under both scenarios (H3A2 and H3B2). The projected ET_0 during the 2030s, 2050s, and 2080s compared to the base period decreased in June, September., and October. months under both scenarios, with the maximum reduction in ET_0 examined in September.

3.4. Future Crop Water Requirement in Potential Climate Scenarios

Crop evapotranspiration (ETc) is closely correlated with ET_0. It indicates the quantity of water a type of plant needs during crop development. Considering the projected ET_0 and present Kc values, the crop water requirement was estimated for cotton, *onion*, soybean, and *sugarcane* for three stations (Pune, Rahuri, and Solapur) for the 2030s, 2050s, and 2080s periods. The water requirements of the four crops were different due to the varied growing periods and Kc values. The CWR was calculated for a three-time period considering both the H3A2 and H3B2 scenarios.

3.4.1. Cotton

Considering both scenarios, the predicted ET_0 in the earlier section revealed that reference evaporation (ET_0) increased for all months except June to September (Kharif Season). Therefore, it is obvious that the water

requirement of cotton would decrease or most likely be the same as that of the base period. Figure 7 represents the variation in CWR of cotton during different periods for all three stations. The base period water requirement of cotton for the Pune station is 620.2 mm. The CWR would marginally decrease during the 2030s and 2050s compared to the present condition.

In the 2080s, a marginal increase of 626.1 mm under H3A2 and 622.1 mm under H3B2 scenarios would be observed for the Pune station. For Rahuri station, the base period CWR is 672.3 mm, which would relatively increase by 4.8 mm and 4 mm for the 2030s and 2080s periods, respectively, and find a relative decrease during the 2050s (-4.5 mm) under the H3A2 scenario. The Solapur station witnesses a higher CWR (717.6 mm) for a base period compared to Rahuri and Pune stations. The CWR for Solapur station would increase during all three periods under both scenarios. (Doria et al., 2006) compared results of estimated CWR to the base period and observed an increase in CWR by 3.0% (20 mm) per season for the 2020s and about 7.0% (43 mm) per season for the 2050s using both H3A2 and H3B2 scenarios.

The CWR would be approximately the same (less than 1% variation) during the 2030s, 2050s, and 2080s concerning the base period for Pune and Rahuri stations. In contrast, it would marginally increase (0.91 to 2.48% variation) for all periods at Solapur station.

3.4.2. Onion

The base/observed period CWR of the onion for the Pune station is 428.9 mm. The CWR would relatively increase by 6.3, 18.1, and 17.9mm under the H3A2 scenario and 7.1, 12.9, and 19.9mm under the H3B2 scenario during the 2030s, 2050s, and 2080s, respectively (Fig. 8). The increment in the CWR was due to the increasing trend in ET_0 observed during the growth period from Nov to Feb. Similarly, the base period CWR of the onion for Rahuri is quite identical to Pune station (428.3 mm). The CWR would relatively increase in the 2030s to 437.9 and 429.2 mm under the H3A2 and H3B2 scenarios, respectively. The CWR for Solapur station would marginally increase during the 2030s and find a relatively large increase during the 2050s under both scenarios. In the 2080s period, the CWR of onions would increase to 559.1 mm by 21 mm under H3A2 and 562.1 mm by 24 mm under H3B2 sequentially.

The CWR would advance to all three stations during the 2030s, 2050s, and 2080s. It would marginally increase (0.49 to 2.48%) during the 2030s, whereas the 2050s and 2080s periods would observe the highest increment in CWR (1.80 to 4.62%) for all three stations. The reason could be a predominant increase in the ET_0 during the winter season under both scenarios.

3.4.3. Soybean

Fig. 9 represents the changes in the CWR of soybean during different periods for all three stations. For the Pune station, the CWR under the H3A2 scenario would marginally decrease by-1.05, -1.05, and -0.16 % during the 2030s, 2050s, and 2080s, respectively. Similarly, CWR would show variation in the range of 1.67 to 0.06% compared to a base period under the H3B2 scenario. The Rahuri station corresponded to a similar variation as the Pune station, from -2.09 to 0.37%. The CWR of soybean for Solapur station would marginally increase or approximately be the same during all three periods (the 2030s, 2050s, and 2080s) under both scenarios. The

CWR would show an increment of up to 1.63% during the 2080s. (Manasa and Shivapur 2016) observed both a rise and a fall in CWR for the future scenario compared with a base period with a decrease in CWR during Kharif crops (sorghum, maize, groundnut, soybean, cotton) and an increase in CWR during rabi crops (sugarcane and wheat).

3.4.4. Sugarcane

Sugarcane has the highest increase in crop water requirements as compared to cotton, onions, and soybeans. The base/observed period CWR of sugarcane for the Pune station is 1384.6 mm. The highest increment in CWR of sugarcane would be during the 2080s, with estimated CWR values of 1421.4 and 1410.8 mm under the H3A2 and H3B2 scenarios, respectively (Fig. 10). The CWR for Rahuri station would be relatively increased in the 2030s to 1460.6 and 1452.8 mm under the H3A2 and H3B2 scenarios, respectively.

Compared to a base period, the 2080s period could observe an increase of 41.1 mm and 24.8 mm under the H3A2 and H3B2 scenarios. For Solapur station, the CWR of sugarcane under the H3A2 would relatively increase during the 2030s (1.66%) and 2050s (1.83%) and increase during the 2080s (2.26%). Similarly, under the H3B2 scenario, the increment in CWR during the 2030s, 2050s, and 2080s would be 1.37, 2.37, and 2.86%, respectively.

4. Discussions

Western Maharashtra, located in the semi-arid zone of India, is a core region for the economic growth of Maharashtra state. The area has an arid climate and minimal water supply and is one of the most fragile ecological environments in the country. The geographical area of the state of Maharashtra is 30.7 Mha, and the cultivable area is 22.5 Mha. Therefore, to optimize water resources management to achieve sustainable development in the region, it is critical to explore the requirements for CWR. At the same time, it is also inevitable to estimate the crop coefficient (Kc) of different parts.

SDSM is used to downscale and project long-term (the 2030s, 2050s, and 2080s) future scenarios of ET_0 from predictors of HadCM3 models in the Western Maharashtra region, India. The H3A2 and H3B2 forcing emission scenarios generated the future ET_0 series. The monthly SDSM sub-model is found to be effective in downscaling ET_0. SDSM projects an increase in mean annual ET_0 for future periods under both scenarios. The annual ET_0 ranges from 0.42 to 3.09%, 0.77 to 3.52%, and 1.54 to 3.13% for Pune, Rahuri, and Solapur stations, respectively. The highest increase in projected monthly ET_0 reached 8.57%, and the decrease approached − 9.15% in Pune. Similarly, the maximum positive increment in projected monthly ET_0 reaches 12.39%, and the decrease is -6.49% at Rahuri station. As for Solapur station, the relative changes range from − 8.09–8.93%, indicating a trend of increase concerning the projected climate change. The uncertainty in future ET_0 projections due to GCMs, emission scenarios, and different time stages is maximized. The results in section 3.3 of this paper show that despite an increasing trend in annual ET_0 during a future period, the ET_0 would drastically decrease in some months. The projected changes in ET_0 revealed that all months during three future periods (the 2030s, 2050s, and 2080s) showed an increment in ET_0 compared to a base period. The ET_0 would advance during summer, pre-monsoon, and winter, whereas it could decrease during the monsoon (Kharif) season. This further implies a decrease in CWR of Kharif crops (cotton and soybean). The CWR would be equal to or less than that of the present condition. Alternatively, the CWR of the rabi crop (onion) shows a phenomenal increase of up to 4.62%.

The perennial crop sugarcane corresponds to a marginal increase in water requirements in the range of 0.05 to 2.86%.

Any of the shortcomings of this research may be the subjects of future investigations. Even though SDSM is a versatile tool in the downscaling method, it does not have any physical significance, and the extent of parameter changes is unknown. Since ET_0 plays a vital role in the hydrological cycle, numerous studies have concentrated on researching ET_0 variability and analyzed that ET_0 is shifting periodically (Bandyopadhyay et al., 2009; Chattopadhyay and Hulme, 1997; Zeng et al., 2019). If there is a loop in CWR at this point, whether or not the future CWR will have the same cycle is not considered. There is also a cascade of ambiguity in the climate change impact analysis, including uncertainty arising from GCMs, emission scenarios, the hydrological model, and the parameters (Wilby and Harris, 2006; Xu et al., 2013). To overcome this uncertainty analysis should be done considering more than one GCM, this would give a better synoptic view of understanding the variability of any climatic parameter under different GCMs.

However, it must be understood that such findings are very much based on the existence of potential climate forecasts and the approaches to GCM used in this research. When large datasets are available, a more sophisticated downscaling method should be used, as different methods will generate different future climate predictions (Chiew et al., 2010; Xu et al., 2013).

5. Conclusion

Many researchers have pointed out that fluctuations in ET_0 have dramatically shifted as climate change has escalated. In the present study, we selected Western Maharashtra to analyze variability in CWR by downscaling ET_0. The SDSM performs satisfactorily in downscaling ET_0 with values of more than 0.60 for R2 and *Ens* and less than 1.32 and 18% for RMSE and MAPE, respectively, during calibration and validation periods. The projected changes showed an increase in ET_0 for all months (in summer, winter, and pre-monsoon seasons) and a decrease from June to September (monsoon season) during the 2030s, 2050s, and 2080s periods compared to the base period under both the H3A2 and H3B2 scenarios. The result is a decrease in projected CWR for Kharif season and an increase in CWR for rabi and summer season. The estimated future CWR showed variation in the range for cotton (-0.97–2.48%), soybean (-2.09–1.63%), onion (0.49–4.62%), and sugarcane (0.05–2.86%) during the 2030s, 2050s, and 2080s period compared to present condition for Pune, Rahuri and Solapur stations under both H3A2 and H3B2 scenario. Considering the impact of climate variability on CWR, it is necessary to promote water-saving technologies like drip and sprinkler irrigation systems. Also, promote rain-water conservation and increase groundwater recharge in the Western Maharashtra region to minimize the risk of yield reduction and enhance maximum water availability in the study area due to climatic variability.

Declarations

Declaration of Competing Interest

The authors declare that they have no known competing financial interests or personal relationships that could have appeared to influence the work reported in this paper. The authors did not receive support from any organization for the submitted work.

Data Availability

The dataset supporting this study's findings is available on request from the corresponding author, Shubham Gade. The dataset is not publicly available as it contains information that could compromise the research participant's privacy and consent.

Code Availability

No code is available for the present study.

Compliance with Ethical Standards

This article does not contain any studies with human participants or animals performed by any authors.

Consent to Participate

Informed consent was obtained from all individual participants included in the study.

Consent to Publish

The participant has consented to the submission of the article to the journal.

Conflict of Interest

The author declares no conflict of interest.

Acknowledgments

We appreciate the editors and the reviewers for their constructive suggestions and insightful comments, which helped us improve this manuscript.

References

1. Allen, R.G., Pereira, L.S., Raes, D., Smith, M., 1998. Crop evapotranspiration-Guidelines for computing crop water requirements- FAO Irrigation and drainage paper No. 56. FAO, Rome 91–165.
2. Anandhi, A., Srinivas, V.. V., Nanjundiah, R., Kumar, N., 2008. Downscaling Precipitation to River Basin in India for IPCC SRES Scenarios Using Support Vector Machine. Int. J. Climatol. 28, 401–420. https://doi.org/10.1002/joc.1529
3. Audit, I.S., 2018. Report of the Comptroller and Auditor General of India on Economic Sector, Government of Maharashtra, Report No. 1 of 2018.
4. Bandyopadhyay, A., Bhadra, A., Raghuwanshi, N.S., Singh, R., 2009. Temporal Trends in Estimates of Reference Evapotranspiration over India. J. Hydrol. Eng. 14, 508–515. https://doi.org/10.1061/(asce)he.1943-5584.0000006
5. Chattopadhyay, N., Hulme, M., 1997. Evaporation and potential evapotranspiration in India under conditions of recent and future climate change Evaporation and potential evapotranspiration in India under conditions of recent and future climate change. Agric. For. Meteorol. 87, 55–73. https://doi.org/10.1016/S0168-1923(97)00006-3

6. Chiew, F.H.., Kirono, D.G.., Kent, D.., Frost, A.., Charles, S.., Timbal, B., Nguyen, K.., Fu, G., 2010. Comparison of runoff modeled using rainfall from different downscaling methods for historical and future climates. J. Hydrol. 387, 10–23. https://doi.org/10.1016/j.jhydrol.2010.03.025
7. Chu, J.T., Xia, J., Xu, C.Y., Singh, V.P., 2010. Statistical downscaling of daily mean temperature, pan evaporation and precipitation for climate change scenarios in Haihe River, China. Theor. Appl. Climatol. 99, 149–161. https://doi.org/10.1007/s00704-009-0129-6
8. Doria, R., Madramootoo, C.A., Mehdi, B.B., 2006. Estimation of future crop water requirements for 2020 and 2050, using CROPWAT, in: 2006 IEEE EIC Climate Change Technology Conference, EICCCC 2006. https://doi.org/10.1109/EICCCC.2006.277194
9. Duhan, D., Pandey, A., Gahalaut, K.P.S., Pandey, R.P., 2013. Spatial and temporal variability in maximum, minimum and mean air temperatures at Madhya Pradesh in central India. Comptes Rendus - Geosci. 345, 3–21. https://doi.org/10.1016/j.crte.2012.10.016
10. Gade, S., Yadav, J., Shinde, S., More, D., Gadekar, K., 2021. Variability in soil moisture using AMSR-E product-A regional case study in the province of Marathwada division, India. Geol. Ecol. Landscapes. https://doi.org/10.1080/24749508.2021.1943811
11. Gagnon, S., Singh, B., Rousselle, J., Roy, L., 2005. An Application of the statistical downscaling model (SDSM) to simulate climatic data for streamflow modelling in Québec. Can. Water Resour. J. 30, 297–314. https://doi.org/10.4296/cwrj3004297
12. Gebrechorkos, S.H., Hülsmann, S., Bernhofer, C., 2019. Statistically downscaled climate dataset for East Africa. Sci. Data 6. https://doi.org/10.1038/S41597-019-0038-1
13. Gebremeskel, S., Liu, Y.B., DeSmedt, F., Hoffmann, L., Pfister, L., 2004. Analysing the effect of climate changes on streamflow using statistically downscaled GCM scenarios. Int. J. River Basin Manag. 2, 271–280. https://doi.org/10.1080/15715124.2004.9635237
14. Goroshi, S., Pradhan, R., Singh, R.P., Singh, K.K., Parihar, J.S., 2017. Trend analysis of evapotranspiration over India: Observed from long-term satellite measurements. J. Earth Syst. Sci. 126, 1–21. https://doi.org/10.1007/s12040-017-0891-2
15. Goyal, R.K., 2004. Sensitivity of evapotranspiration to global warming: A case study of arid zone of Rajasthan (India). Agric. Water Manag. 69, 1–11. https://doi.org/10.1016/j.agwat.2004.03.014
16. Guhathakurta, P., Khedikar, S., Menon, P., Prasad, A.K., Sable, S.T., Advani, S.C., 2020. CLIMATE RESEARCH AND SERVICES Observed Rainfall Variability and Changes over Maharashtra State.
17. Guo, B., Zhang, J., Xu, T., 2018. Comparison of two statistical climate downscaling models: a case study in the Beijing region, China. Int. J. Water 12, 22–38. https://doi.org/10.1504/IJW.2018.090186
18. Huang, J., Zhang, J., Zhang, Z., Xu, C., Wang, B., Yao, J., 2011. Estimation of future precipitation change in the Yangtze River basin by using statistical downscaling method. Stoch Env Res Risk A 25, 781–792. https://doi.org/10.1007/s00477-010-0441-9
19. Hussain, M., Yusof, K.W., Mustafa, M.R., Afshar, N.R., 2015. Application of statistical downscaling model (SDSM) for long term prediction of rainfall in Sarawak, Malaysia. Water Resour. Manag. VIII 1, 269–278. https://doi.org/10.2495/WRM150231
20. IPCC, 2013. The Physical Science Basis. Contribution of Working Group I to the Fifth Assessment Report of the Intergovernmental Panel on Climate Change. Cambridge University Press, Cambridge, United Kingdom

and New York, NY, USA. https://doi.org/10.1017/CBO9781107415324

21. IPCC, 2007. The Physical Science Basis. Contribution of Working Group I to the Fourth Assessment Report of the Intergovernmental Panel on Climate Change. Cambridge University Press, Cambridge, United Kingdom and New York, NY, USA, pp. 214–219.
22. IPCC, 2002. Climate change and biodiversity. Geneva, Switzerland.
23. Khan, M.S., Coulibaly, P., Dibike, Y., 2006. Uncertainty analysis of statistical downscaling methods. J. Hydrol. 319, 357–382. https://doi.org/10.1016/j.jhydrol.2005.06.035
24. Kranz, N., Menniken, T., Hinkel, J., 2010. Climate change adaptation strategies in the Mekong and Orange-Senqu basins : What determines the state-of-play? Environ. Sci. Policy 13, 648–659. https://doi.org/10.1016/j.envsci.2010.09.003
25. Kumar, S., 2007. Fourth assessment report of the Intergovernmental Panel on Climate Change: Important observations and conclusions. Curr. Sci.
26. Kundu, S., Khare, D., Mondal, A., 2017. Future changes in rainfall, temperature and reference evapotranspiration in the central India by least square support vector machine. Geosci. Front. 8, 583–596. https://doi.org/10.1016/j.gsf.2016.06.002
27. Mahmood, R., Babel, M.S., 2013. Evaluation of SDSM developed by annual and monthly sub-models for downscaling temperature and precipitation in the Jhelum basin, Pakistan and India. Theor. Appl. Climatol. 113, 27–44. https://doi.org/10.1007/s00704-012-0765-0
28. Manasa, H.G., Shivapur, A.V., 2016. Implications of Climate Change on Crop Water Requirements in Hukkeri Taluk of Belagavi District, Karnataka, India. Int. J. Res. Eng. Technol. 05, 236–241. https://doi.org/10.15623/ijret.2016.0506044
29. Micheal, A.M., 2008. Irrigation: Theory and Practices, 2nd ed. Vikas Publishing House Pvt, Ltd., New Delhi.
30. Mohan, S., Ramsundram, N., 2014. Change and its Impact on Irrigation Water Requirements on Temporal Scale. Irrig. Drain. Sys Eng 3. https://doi.org/10.4172/2168-9768.1000118
31. Pandey, R.P., Dash, B.B., Mishra, S.K., Singh, R., 2008. Study of indices for drought characterization in KBK districts in Orissa (India). Hydrol. Process 22, 1895–1907. https://doi.org/10.1002/hyp.6774
32. Rajabi, A., Babakhani, Z., 2018. The study of potential evapotranspiration in future periods due to climate change in west of Iran. Int. J. Clim. Chang. Strateg. Manag. 10, 161–177. https://doi.org/10.1108/IJCCSM-01-2017-0008
33. Saraf, V.R., Regulwar, D.G., 2016. Assessment of Climate Change for Precipitation and Temperature Using Statistical Downscaling Methods in Upper Godavari River Basin, India. J. Water Resour. Prot. 08, 31–45. https://doi.org/10.4236/jwarp.2016.81004
34. Suo, M.Q., Zhang, J., Zhou, Q., Li, Y.P., 2019. Applicability analysis of SDSM technology to climate simulation in Xingtai City, China. IOP Conf. Ser. Earth Environ. Sci. 223. https://doi.org/10.1088/1755-1315/223/1/012053
35. Tamaddun, K.A., Kalra, A., Bernardez, M., Ahmad, S., 2019. Effects of ENSO on temperature, precipitation, and potential evapotranspiration of north India's monsoon: An analysis of trend and entropy. Water (Switzerland) 11. https://doi.org/10.3390/w11020189
36. Tao, X. e., Chen, H., yu Xu, C., kun Hou, Y., xuan Jie, M., 2015. Analysis and prediction of reference evapotranspiration with climate change in Xiangjiang River Basin, China. Water Sci. Eng. 8, 273–281.

https://doi.org/10.1016/j.wse.2015.11.002
37. TERI, 2014. Assessing climate change vulnerability and adaptation strategies for Maharashtra: Maharashtra State Adaptation Action Plan on Climate Change (MSAAPC) New Delhi: The Energy and Resources Institute.
38. Thomas, A., 2008. Agricultural irrigation demand under present and future climate scenarios in China. Glob. Planet. Change 60, 306–326. https://doi.org/10.1016/j.gloplacha.2007.03.009
39. Wang, F., Chen, Y., Li, Z., Fang, G., Li, Y., Xia, Z., 2019. Assessment of the irrigation water requirement and water supply risk in the Tarim River Basin, Northwest China. Sustain. 11. https://doi.org/10.3390/su11184941
40. Wang, W., Xing, W., Shao, Q., Yu, Z., Peng, S., Yang, T., Yong, B., Taylor, J., Singh, V.P., 2013. Changes in reference evapotranspiration across the Tibetan Plateau: Observations and future projections based on statistical downscaling. J. Geophys. Res. Atmos. 118, 4049–4068. https://doi.org/10.1002/jgrd.50393
41. Wilby, R.., Dawson, C.., Barrow, E.., 2002. SDSM—A Decision Support Tool for the Assessment of Regional Climate Change Impacts. Environ. Model. Softw. 17, 147–159. https://doi.org/10.1016/S1364-8152(01)00060-3
42. Wilby, R.L., Dawson, C.., 2007. SDSM 4.2 – A decision support tool for the assessment of regional climate change impacts.
43. Wilby, R.L., Harris, L., 2006. A framework for assessing uncertainties in climate change impacts: Low-flow scenarios for the river Thames, UK. Water Resour. Res. 42. https://doi.org/10.1029/2005WR004065
44. Wilby, R.L., Wigley, T.M.L., 2000. Precipitation predictors for downscaling: Observed and general circulation model relationships. Int. J. Climatol. 20, 641–661. https://doi.org/10.1002/(SICI)1097-0088(200005)20:6<641::AID-JOC501>3.0.CO;2-1
45. Wilby, R.L., Wigley, T.M.L., 1997. Downscaling general circulation model output: A review of methods and limitations. Prog. Phys. Geogr. 21, 530–548. https://doi.org/10.1177/030913339702100403
46. Xu, Y.P., Pan, S., Fu, G., Xujie, Z., 2014. Future potential evapotranspiration changes and contribution analysis in Zhejiang Province, East China. J. Geophys. Res. Atmos. 118, 2174–2192. https://doi.org/10.1002/2013JD021245.Received
47. Xu, Y.P., Zhang, X., Ran, Q., Tian, Y., 2013. Impact of climate change on hydrology of upper reaches of Qiantang River Basin, East China. J. Hydrol. 483, 51–60. https://doi.org/10.1016/j.jhydrol.2013.01.004
48. Zeng, Z., Wu, W., Zhou, Y., Li, Z., Hou, M., Huang, H., 2019. Changes in reference evapotranspiration over Southwest China during 1960-2018: Attributions and implications for drought. Atmosphere (Basel). 10. https://doi.org/10.3390/atmos10110705
49. Zhai, P., Zhang, Z., Wan, H., Pan, X., 2005. Trends in Total Precipitation and Frequency of Daily Precipitation Extremes over China. J. Clim. 18, 1096–1108. https://doi.org/10.1175/JCLI-3318.1
50. Zhou, T., Wu, P., Sun, S., Li, X., Wang, Y., Luan, X., 2017. Impact of future climate change on regional crop water requirement-A case study of Hetao irrigation district, China. Water (Switzerland) 9. https://doi.org/10.3390/w9060429
51. Zotarelli, L., Dukes, M.., Romero, C.., Migliaccio, K.., Morgan, T.., 2010. Step by Step Calculation of the Penman-Monteith Evapotranspiration (FAO-56 Method). Agric. Biol. Eng.

Figures

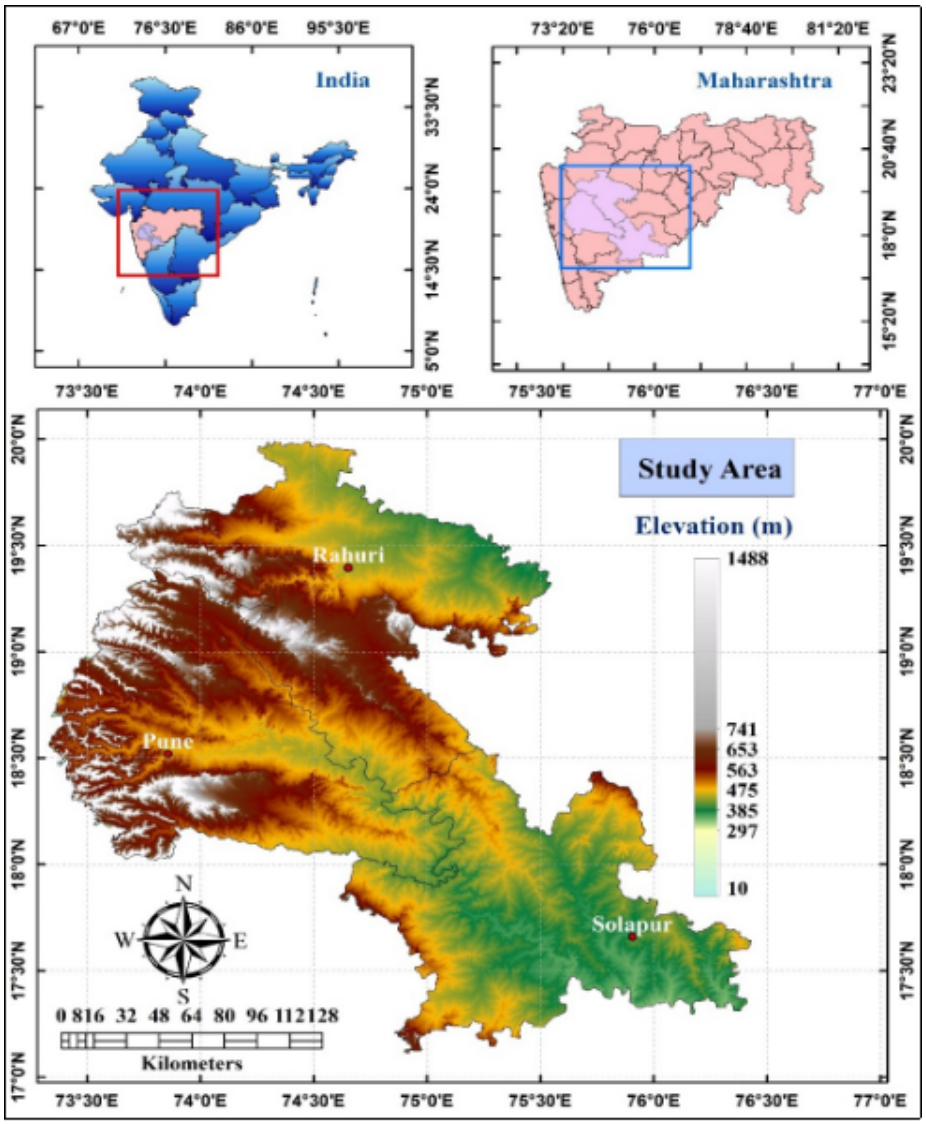

Figure 1. The location map of Western Maharashtra

Figure 1

The location map of Western Maharashtra

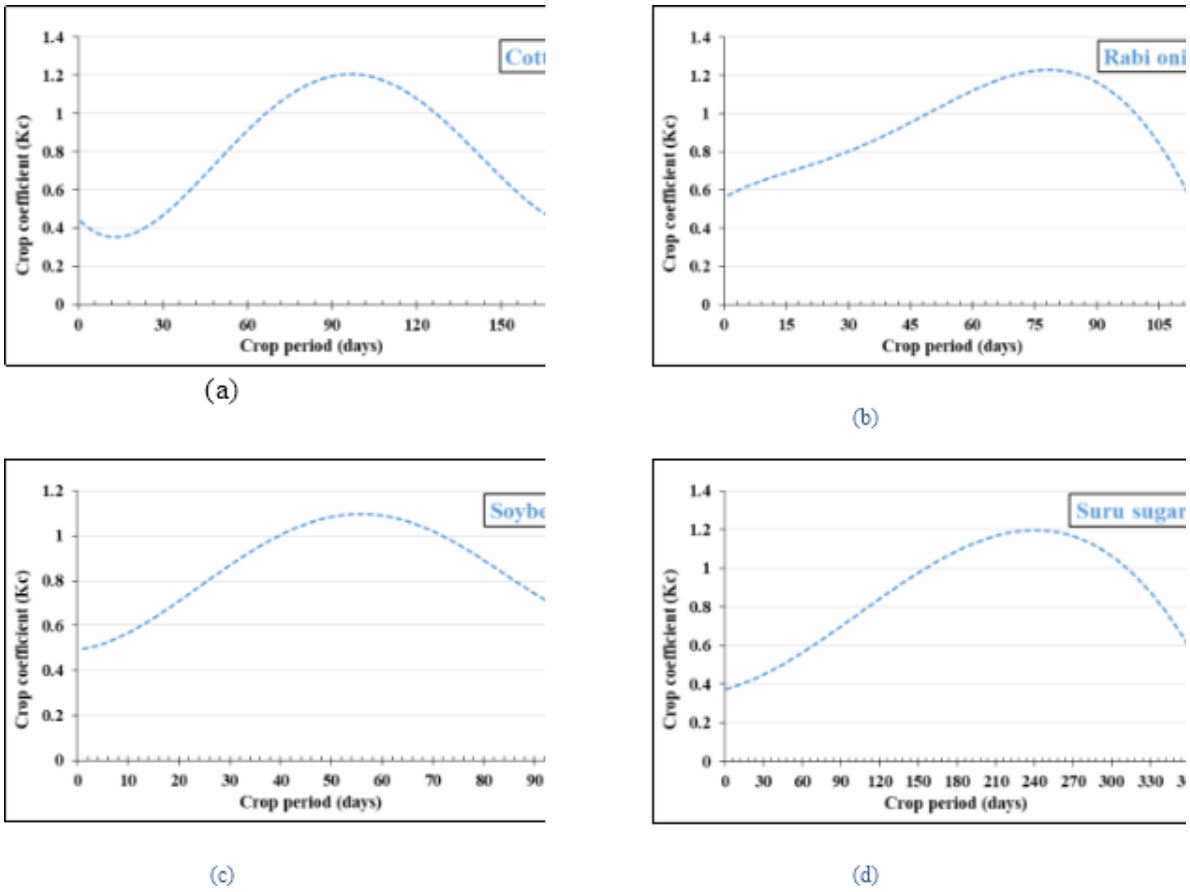

Figure 2

Crop coefficient K_c curve during growth stage for a) Cotton, b) Onion, c) Soybean, and d) Sugarcane

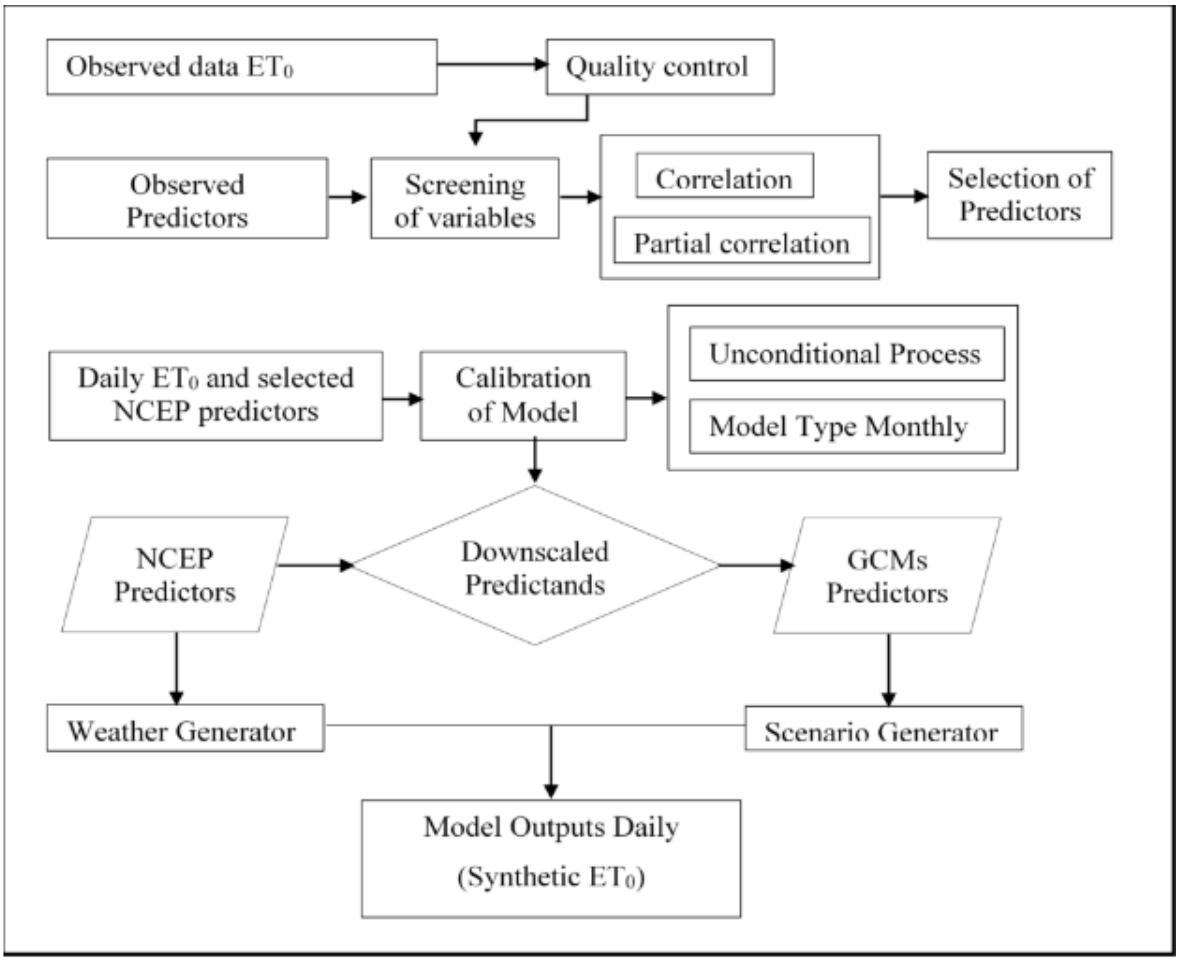

Figure 3. Flow chart showing depicting involved during downscaling and scenario generation modified after (Saraf and Regulwar, 2016; Wilby and Dawson, 2007)

Figure 3

Flow chart showing depicting involved during downscaling and scenario generation modified after (Saraf and Regulwar, 2016; Wilby and Dawson, 2007)

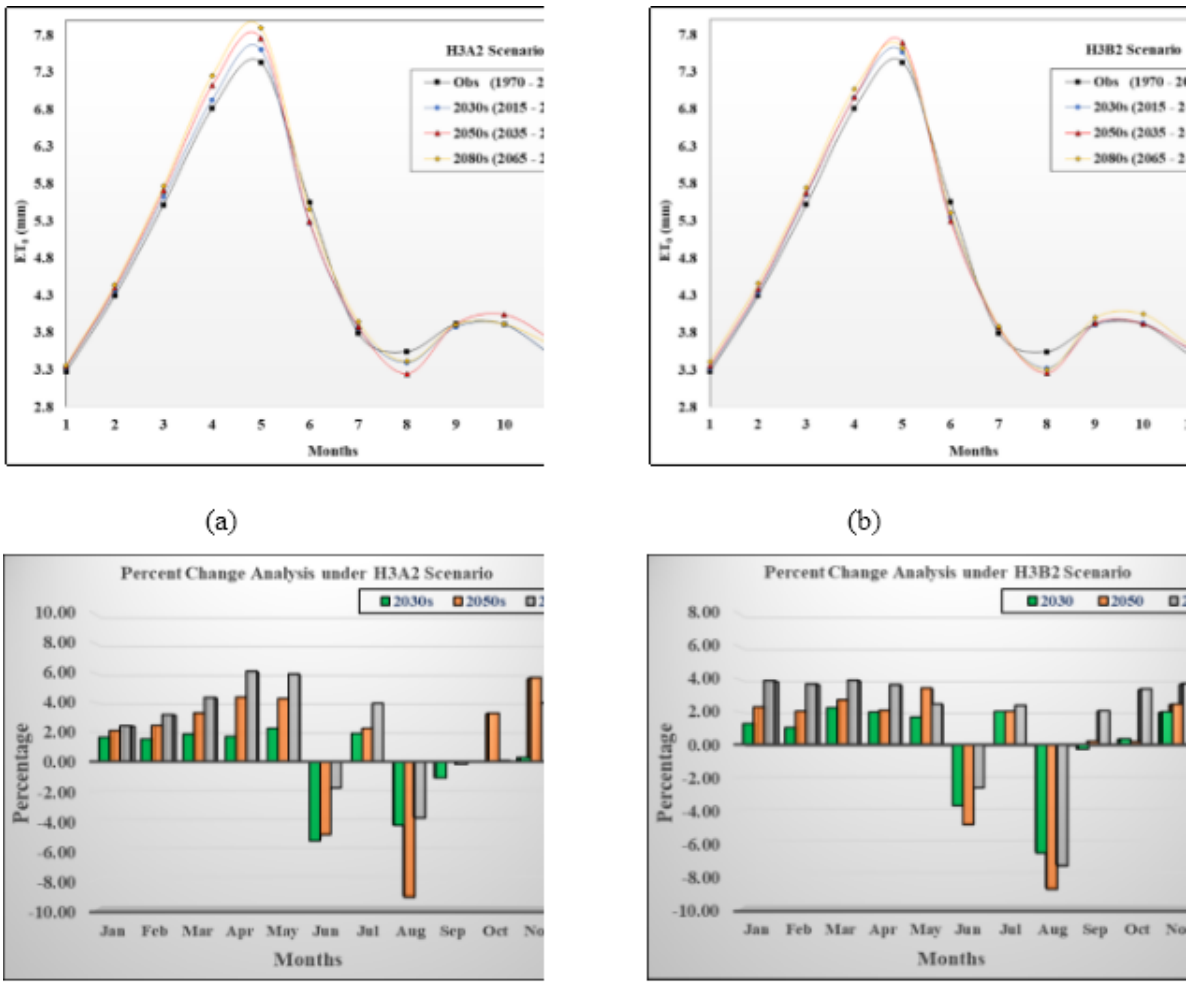

Figure 4

Mean monthly downscaled ET_0 under (a) H3A2 and (b) H3B2 scenario; and percent changes in ET_0 as compared to base period under (c) H3A2 and (d) H3B2 scenario for Pune station

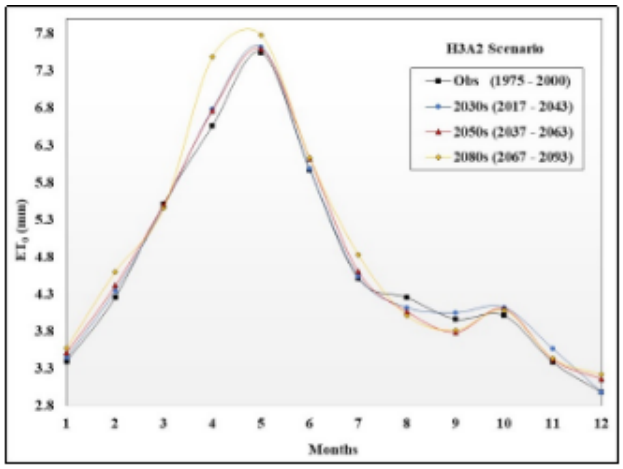

(a)

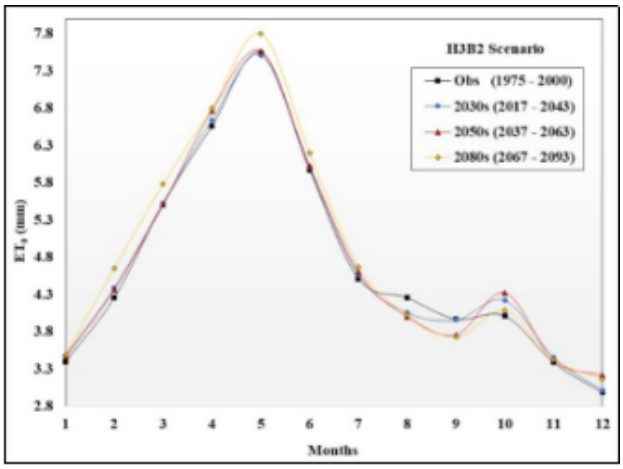

(b)

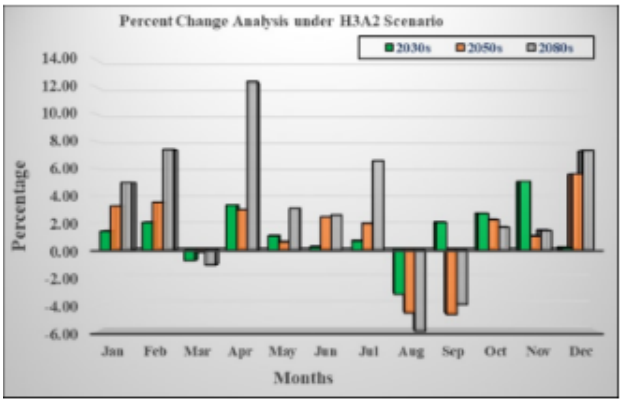

(c)

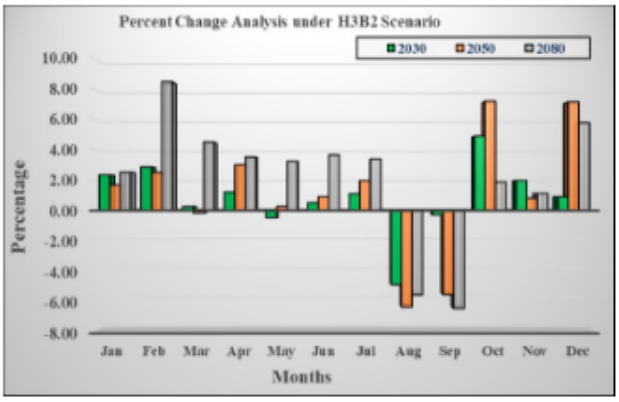

(d)

Figure 5

Mean monthly downscaled ET_0 under (a) H3A2 and (b) H3B2 scenario; and percent changes in ET_0 as compared to base period under (c) H3A2 and (d) H3B2 scenario for Rahuri station

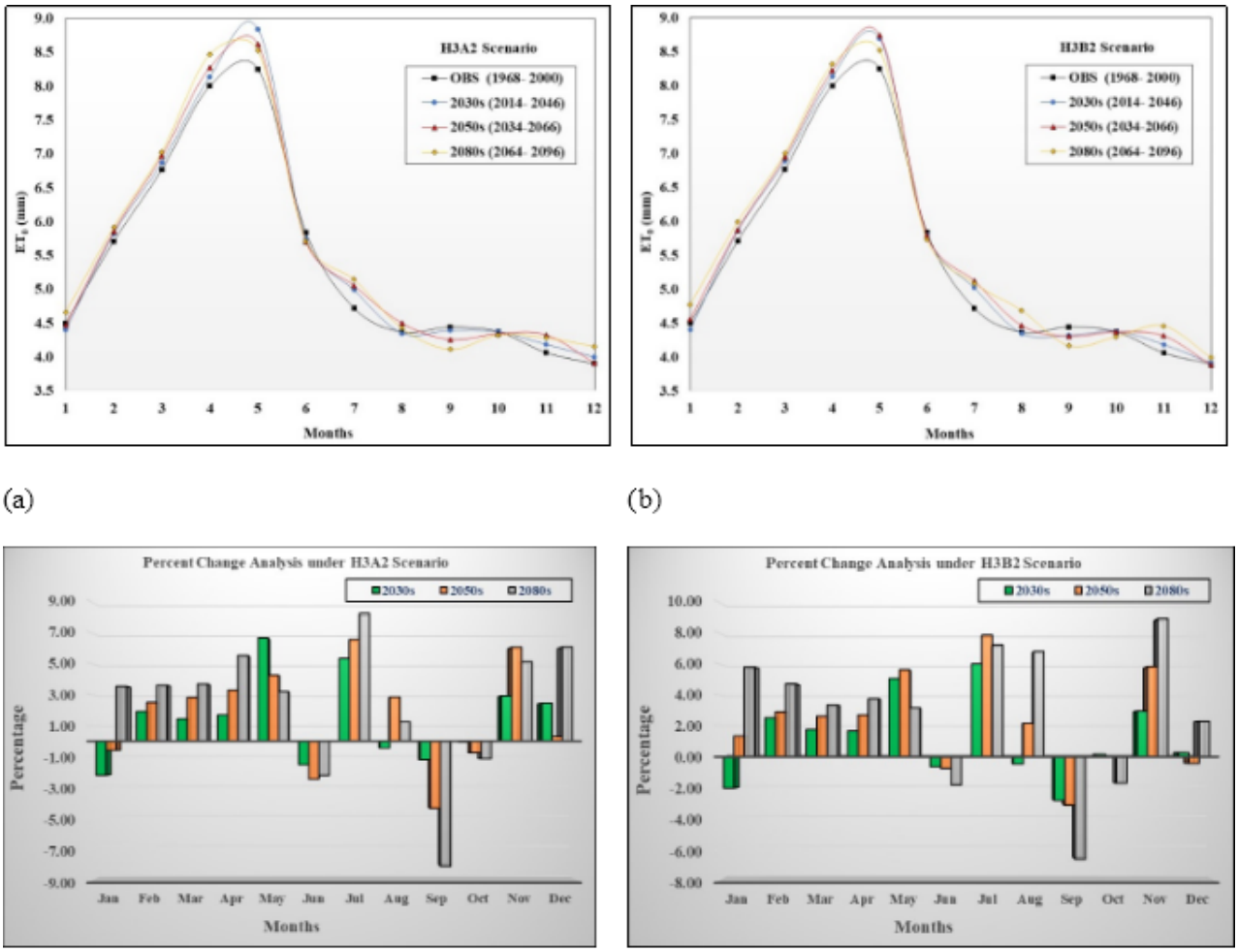

Figure 6

Mean monthly downscaled ET_0 under (a) H3A2 and (b) H3B2 scenario; and percent changes in ET_0 as compared to base period under (c) H3A2 and (d) H3B2 scenario for Solapur station

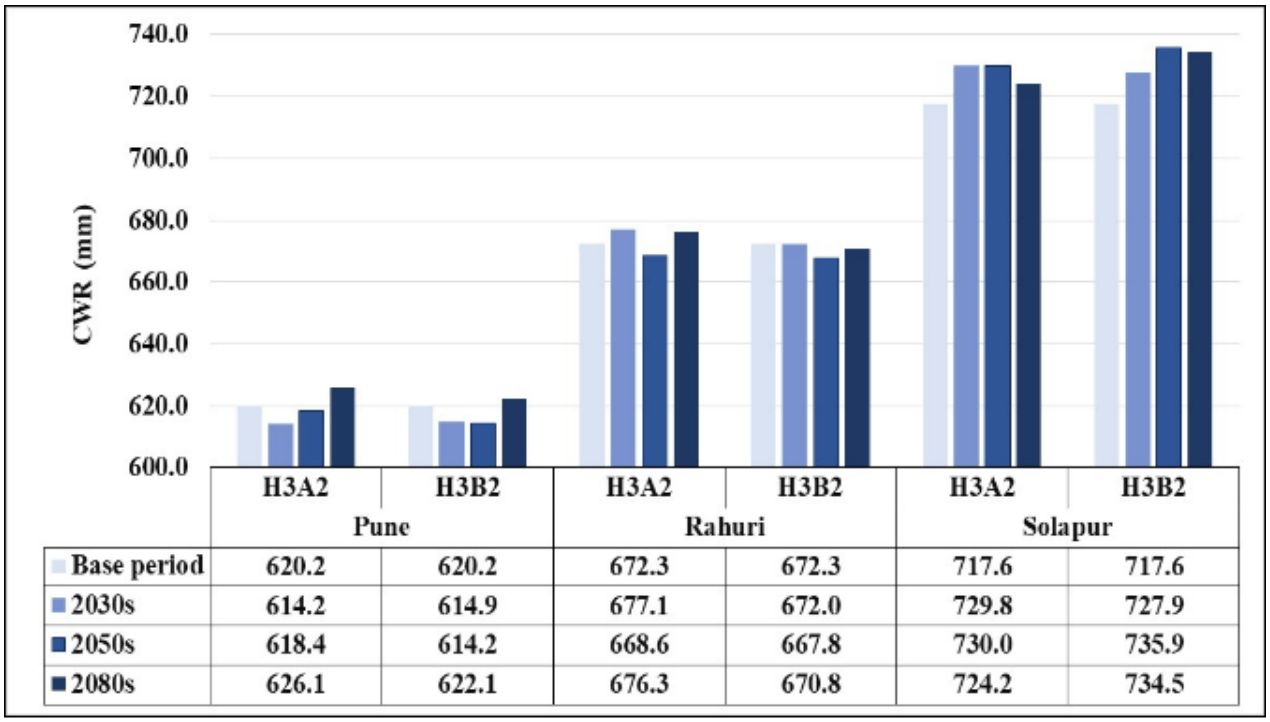

	H3A2	H3B2	H3A2	H3B2	H3A2	H3B2
	Pune		Rahuri		Solapur	
Base period	620.2	620.2	672.3	672.3	717.6	717.6
2030s	614.2	614.9	677.1	672.0	729.8	727.9
2050s	618.4	614.2	668.6	667.8	730.0	735.9
2080s	626.1	622.1	676.3	670.8	724.2	734.5

Figure 7. CWR of cotton during different time period at different stations

Figure 7

CWR of cotton during different time period at different stations

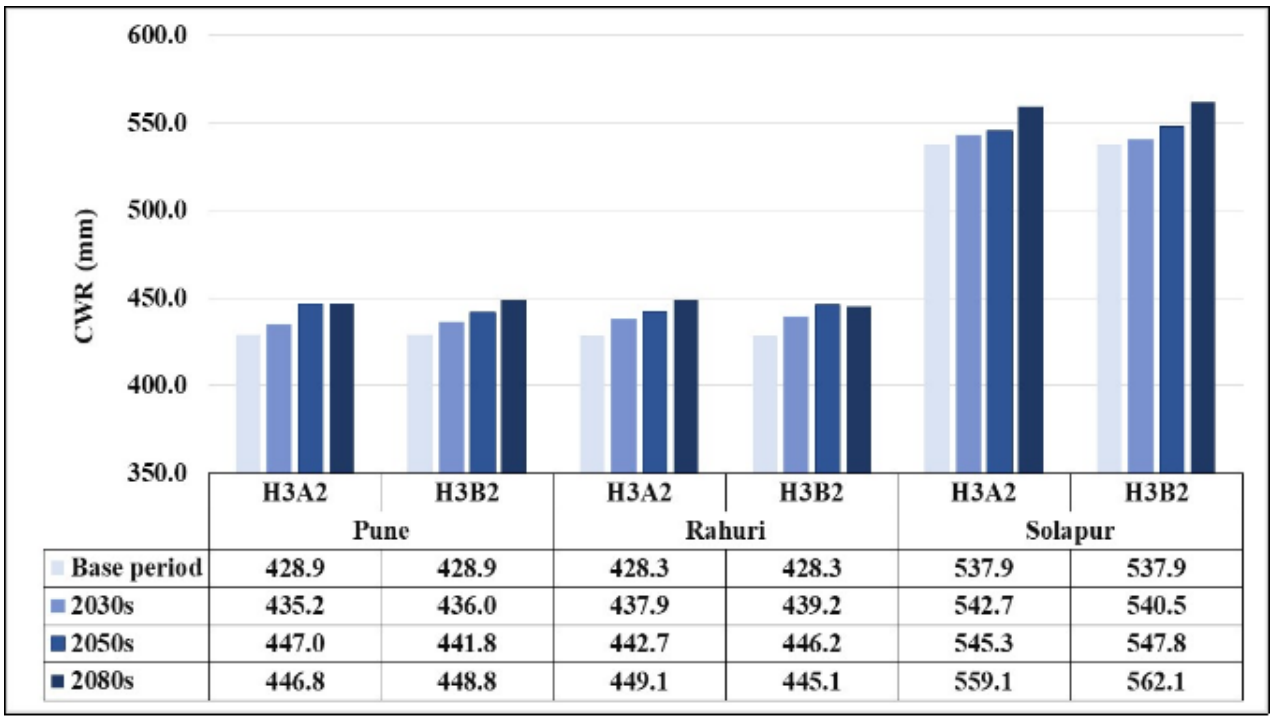

	H3A2	H3B2	H3A2	H3B2	H3A2	H3B2
	Pune		Rahuri		Solapur	
Base period	428.9	428.9	428.3	428.3	537.9	537.9
2030s	435.2	436.0	437.9	439.2	542.7	540.5
2050s	447.0	441.8	442.7	446.2	545.3	547.8
2080s	446.8	448.8	449.1	445.1	559.1	562.1

Figure 8. CWR of *onion* during different time period at different stations

Figure 8

CWR of *onion* during different time period at different stations

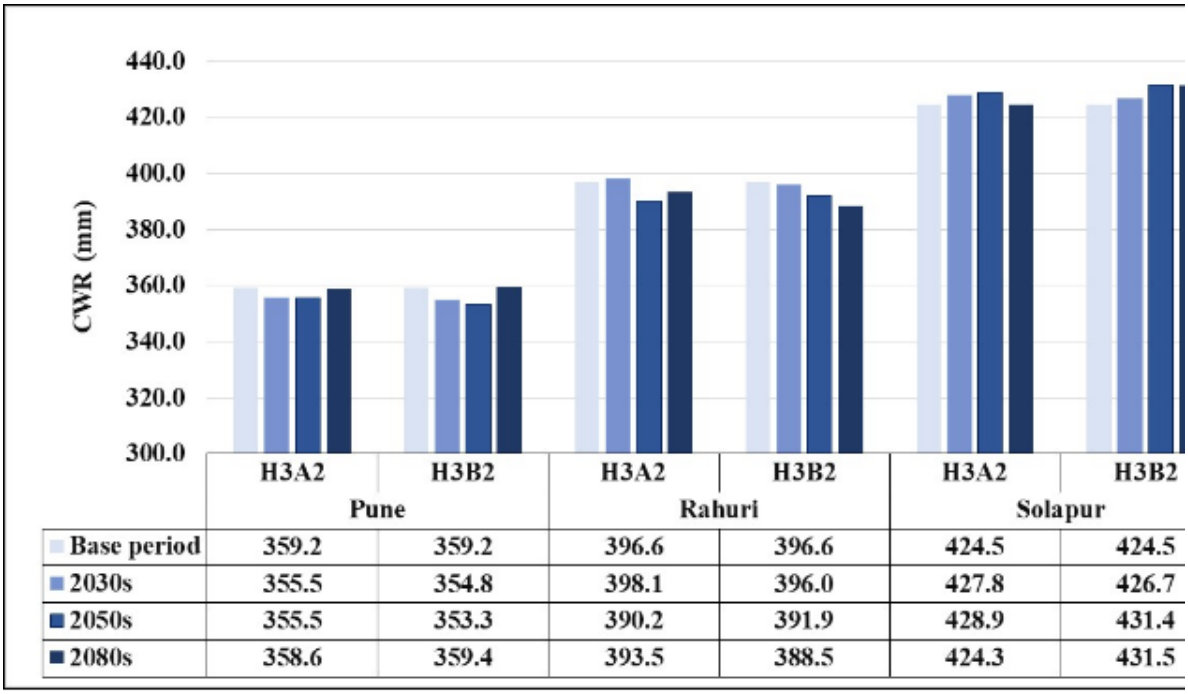

	H3A2	H3B2	H3A2	H3B2	H3A2	H3B2
	Pune		Rahuri		Solapur	
Base period	359.2	359.2	396.6	396.6	424.5	424.5
2030s	355.5	354.8	398.1	396.0	427.8	426.7
2050s	355.5	353.3	390.2	391.9	428.9	431.4
2080s	358.6	359.4	393.5	388.5	424.3	431.5

Figure 9. CWR of soybean during different time period at different stations

Figure 9

CWR of soybean during different time period at different stations

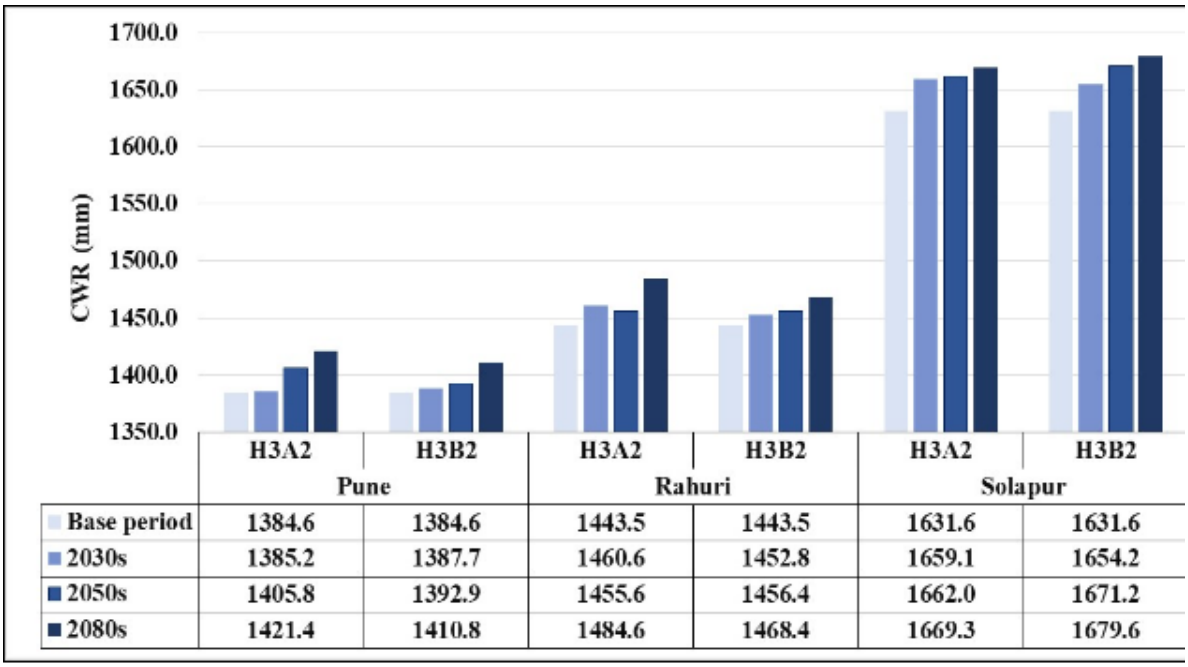

	H3A2	H3B2	H3A2	H3B2	H3A2	H3B2
	Pune		Rahuri		Solapur	
Base period	1384.6	1384.6	1443.5	1443.5	1631.6	1631.6
2030s	1385.2	1387.7	1460.6	1452.8	1659.1	1654.2
2050s	1405.8	1392.9	1455.6	1456.4	1662.0	1671.2
2080s	1421.4	1410.8	1484.6	1468.4	1669.3	1679.6

Figure 10. CWR of *sugarcane* during different time period at different stations

Figure 10

CWR of *sugarcane* during different time period at different stations